Density-functional theory simulation of large quantum dots

Hong Jiang,[1,2,3] Harold U. Baranger,[2,*] and Weitao Yang[1,†]
[1]*Department of Chemistry, Duke University, Durham, North Carolina 27708-0354, USA*
[2]*Department of Physics, Duke University, Durham, North Carolina 27708-0305, USA*
[3]*College of Chemistry and Molecular Engineering, Peking University, Beijing 100871, China*
(Received 7 January 2003; revised manuscript received 2 June 2003; published 24 October 2003)

Kohn-Sham spin-density functional theory provides an efficient and accurate model to study electron-electron interaction effects in quantum dots, but its application to large systems is a challenge. Here an efficient method for the simulation of quantum dots using density-function theory is developed; it includes the particle-in-the-box representation of the Kohn-Sham orbitals, an efficient conjugate-gradient method to directly minimize the total energy, a Fourier convolution approach for the calculation of the Hartree potential, and a simplified multigrid technique to accelerate the convergence. We test the methodology in a two-dimensional model system and show that numerical studies of large quantum dots with several hundred electrons become computationally affordable. In the noninteracting limit, the classical dynamics of the system we study can be continuously varied from integrable to fully chaotic. The qualitative difference in the noninteracting classical dynamics has an effect on the quantum properties of the interacting system: integrable classical dynamics leads to higher-spin states and a broader distribution of spacing between Coulomb blockade peaks.

DOI: 10.1103/PhysRevB.68.165337 PACS number(s): 73.21.La, 71.15.Dx, 31.15.Ew

I. INTRODUCTION

A semiconductor quantum dot (QD) is a kind of nanodevice in which the motion of electrons is quantized in all three dimensions through the lateral confinement of a high-mobility modulation-doped two-dimensional (2D) electron gas in a semiconductor heterostructure.[1–4] Both quantum interference and electron-electron interactions play important roles in quantum dots, and their interplay underlies many properties that are fascinating in terms of both fundamental mesoscopic physics and future technical applications. Various theoretical models have been developed to explain experimental discoveries and to predict new properties.[2,4] The Kohn-Sham (KS) density-functional theory (DFT) method[5–7] provides an accurate numerical model to study electron-electron interaction effects in QD systems.[8–19] In spite of its comparatively low computational cost, previous DFT calculations are limited to systems in which the electron number is generally less than a few tens. In many experimental cases, however, the electron numbers involved are more than several hundreds. The main theoretical approaches in the regime of large number of electrons are statistical methods[2,3,20,21] which are usually based on some general assumptions whose validity, in many cases, is yet to be justified. It is therefore desirable to explore the large dot regime directly by using numerically more accurate models such as DFT. This imposes a demanding computational task because to obtain meaningful statistics, many calculations with several hundred electrons need to be done. It is therefore compelling to develop more efficient numerical techniques for DFT simulation of QD systems.

Two key issues are involved in the numerical implementation of the KS-DFT method:[22,23] (1) the numerical representation of wave functions and the KS Hamiltonian and (2) the solution of the numerical KS equation. While local basis sets (mainly Gaussian-type orbitals) dominate in conventional quantum chemistry of molecular systems,[24] the plane-wave (PW) basis,[22,23] combined with the pseudopotential method, is widely used in the *ab initio* electronic calculations of various material systems, in which the fast-Fourier-transform (FFT) method can be used to take full advantage of the periodicity of crystal structures. In principle, the PW method is valid only for periodic systems, but aperiodic systems can be treated by introducing the supercell technique.[22] In recent years, several groups have been advocating the use of basis-free real-space methods for electronic structure calculations of finite systems, in which the wave functions are represented in real space, and the kinetic-energy operator is discretized by a high-order finite-difference (FD) method.[25] With a given representation, there are various methods to solve the resultant numerical KS equation.[22,23] Roughly they fall into two different types: methods that minimize the total energy directly,[22,23] and those that solve the KS equation in a self-consistent way.[23] In addition, for DFT simulations of finite systems, another important issue is the calculation of the Hartree potential.[26–29]

Aiming at modeling QD systems efficiently, we have developed techniques in both the numerical representation of KS orbitals and the solution of the KS equation. We note that in QD systems, the wave functions vanish at the boundaries, and in some cases even hard-wall boundary conditions are used. For a function in a rectangular box with zero boundary values, the most natural basis set is the particle-in-the-box (PiB) basis set. The kinetic-energy operator is diagonal in the PiB space and the transformation between real and PiB space can be efficiently performed by the fast-sine-transform (FST) method, which is a variant of the FFT. For the solution of the KS equation, we modified Teter, Payne, and Allan's (TPA's) band-by-band conjugate-gradient method[30,22] to get a more efficient direct-minimization approach.

The methodology developed in this paper is equally applicable to systems of any dimension, but since quantum dots are usually approximated as ideally 2D systems,[4] we will report our numerical results only for 2D systems. In our previous study,[19] this methodology was used to investigate statistics of conductance peak spacing and ground-state spin in

large quantum dots with electron number N up to 200. In this paper, we extend the calculations for even larger dots with N up to 400, which makes it possible to investigate the interplay between classical integrability of external potentials and electron-electron interaction. Some results will be presented as an application of the methodology. We find that the nature of the noninteracting classical dynamics does affect the DFT results: integrability leads to a greater fraction of high-spin states and to a broader distribution of Coulomb blockade peak spacings. However, the effect of integrability is smaller than the effect of symmetry of the external potential, indicating that the interactions affect the integrability of the system more easily than its symmetry.

The outline of the paper is as follows. In the following section, after a simple description of the KS-DFT method, we present the main components of our method: (1) the PiB representation of the KS equation; (2) a modified band-by-band conjugate-gradient method for the direct minimization of the KS total energy; (3) a Fourier convolution method for the calculation of the Hartree potential that was developed by Martyna and Tuckerman[29] in the PW pseudopotential calculations; and (4) a simple one-way multigrid technique to accelerate the convergence that was first proposed by Lee *et al.*[31] In Sec. III, our method is tested and evaluated in a 2D model QD with electron number $N=100$. In Sec. IV, this method is applied to study spin and peak-spacing distributions in large integrable and chaotic quantum dots with N up to 400. Finally, Sec. V summarizes the main results and concludes the paper.

II. METHOD

A. Kohn-Sham spin-density functional theory

Considering the important role played by electron spin in QD systems, we take the effect of spin polarization explicitly into account in the framework of Kohn-Sham spin-density functional theory (KS-SDFT).[5,7] In KS-SDFT, the ground-state energy of an interacting system with electron number N and the total spin S in the local external potential $V_{\text{ext}}(\mathbf{r})$ is written as a functional of spin densities n^σ with $\sigma=\alpha,\beta$ denoting spin up and spin down, respectively:

$$E[n^\alpha,n^\beta]=T_s[n^\alpha,n^\beta]+\int n(\mathbf{r})V_{\text{ext}}(\mathbf{r})d\mathbf{r} + \frac{1}{2}\int\int \frac{n(\mathbf{r})n(\mathbf{r}')}{|\mathbf{r}-\mathbf{r}'|}d\mathbf{r}d\mathbf{r}'+E_{\text{xc}}[n^\alpha,n^\beta]. \tag{1}$$

(Effective atomic units are used throughout the paper: for GaAs QD's with an effective electron mass $m^*=0.067m_e$ and a dielectric constant $\epsilon=12.9$, values are 10.96 meV for energy and 10.19 nm for length.) $T_s[n^\alpha,n^\beta]$ is the kinetic energy of the KS noninteracting reference system which has the same ground-state spin density as the interacting one and $E_{\text{xc}}[n^\alpha,n^\beta]$ is the exchange-correlation energy functional. The spin densities n^σ satisfy the constraint $\int n^\sigma(\mathbf{r})d\mathbf{r}=N^\sigma$ with $N^\alpha=(N+2S)/2$ and $N^\beta=(N-2S)/2$.

Assuming that the ground state of the noninteracting reference system is nondegenerate, the noninteracting kinetic energy is given by $T_s[n^\alpha,n^\beta]=\Sigma_{i,\sigma}\langle\psi_i^\sigma|-\frac{1}{2}\nabla^2|\psi_i^\sigma\rangle$, and the ground-state spin density is uniquely expressed as

$$n^\sigma(\mathbf{r})=\sum_i^{N^\sigma}|\psi_i^\sigma(\mathbf{r})|^2,\quad \sigma=\alpha,\beta. \tag{2}$$

Here ψ_i^σ are the lowest single-particle orbitals which are obtained from

$$\mathbf{H}_{\text{KS}}^\sigma\psi_i^\sigma(\mathbf{r})=\varepsilon_i^\sigma\psi_i^\sigma(\mathbf{r}), \tag{3}$$

with the KS Hamiltonian $\mathbf{H}_{\text{KS}}$ defined as

$$\mathbf{H}_{\text{KS}}^\sigma\equiv-\tfrac{1}{2}\nabla^2+V_{\text{ext}}(\mathbf{r})+V_H[n;\mathbf{r}]+V_{\text{xc}}^\sigma[n^\alpha,n^\beta;\mathbf{r}]. \tag{4}$$

$V_H[n;\mathbf{r}]$ and $V_{\text{xc}}^\sigma[n^\alpha,n^\beta;\mathbf{r}]$ are the Hartree and exchange-correlation potentials, respectively:

$$V_H[n;\mathbf{r}]\equiv\int\frac{n(\mathbf{r}')}{|\mathbf{r}-\mathbf{r}'|}d^3\mathbf{r}', \tag{5}$$

$$V_{\text{xc}}^\sigma[n^\alpha,n^\beta;\mathbf{r}]\equiv\frac{\delta E_{\text{xc}}[n^\alpha,n^\beta]}{\delta n^\sigma(\mathbf{r})}. \tag{6}$$

In our calculations, we have used the local spin-density approximation (LSDA) (Refs. 5,7) for E_{xc}. In the 3D cases, the validity of LSDA has been well justified in the modeling of material systems. Although more accurate exchange-correlation functional forms such as the generalized-gradient approximation (GGA) (Refs. 5,32) are available, it has been shown that the GGA results are close to those from LSDA calculations in QD systems.[14] In the cases of 2D systems, several LSDA exchange-correlation functional forms have been developed by parametrizing results obtained from quantum Monte Carlo modeling of 2D electron gas.[33–35] We use Tanatar and Ceperley's parametrized form[33] of 2D LSDA functional for nonpolarized and ferromagnetic limits, and use an exchangelike interpolation formula for intermediate polarization.[4] In terms of the implementation, the calculation of V_{xc} is trivial when the spin densities are in real space as is the case in our algorithm, but the calculation of V_H requires more effort as will be shown later.

B. PiB representation

To simplify the notation, we will take 1D systems as an example, the generalization to higher dimensional cases being straightforward. Any regular function $f(x)$ that is localized in the finite region $0<x<L$ with zero boundary values can be expanded as

$$f(x)=\sum_n C_n\sqrt{\frac{2}{L}}\sin\frac{n\pi x}{L} \tag{7}$$

and the expansion coefficients C_n are

$$C_n=\sqrt{\frac{2}{L}}\int_0^L f(x)\sin\frac{n\pi x}{L}dx. \tag{8}$$

Integrating Eq. (8) numerically on a set of equally spaced discrete points $\{x_j \equiv j\Delta x \equiv j(L/N_x)\}$ using the extended trapezoidal formula[36] leads to

$$C_n = \sqrt{\frac{2}{L}}\Delta x \sum_{j=1}^{N_x-1} f_j \sin\frac{\pi jn}{N_x} = F_n \frac{\sqrt{2L}}{N_x} \tag{9}$$

with $f_j \equiv f(x_j)$ and

$$F_n \equiv \sum_{j=1}^{N_x-1} f_j \sin\frac{\pi jn}{N_x} \equiv \mathbf{FST}\{f_j\}, \tag{10}$$

where $\mathbf{FST}\{f_j\}$ denotes the fast sine transform of the data $\{f_j\}$.

One of the key ingredients in our method is the action of the single-particle Hamiltonian operator on wave functions:

$$\mathbf{H}f(x) = \mathbf{T}f(x) + \mathbf{V}f(x), \tag{11}$$

the efficiency of which is critical for the performance of the whole method. Whereas the potential-energy operator is diagonal in real space, the kinetic-energy operator is diagonal in PiB space. Wave functions can be transformed between the two spaces efficiently by the fast sine transform. In our method, wave functions are in discrete real space $\{f_j\}$, and the application of the potential-energy operator is therefore trivial, $\mathbf{V}\{f_j\} = \{V_j f_j\}$, where V_j is the value of the potential at the point x_j. The kinetic-energy operator is applied to wave functions in PiB space:

$$\mathbf{T}f(x) \equiv -\frac{\hbar^2}{2m}\nabla^2 f(x) = \frac{2}{N_x}\sum_n F_n \frac{\hbar^2 k_n^2}{2m}\sin\frac{n\pi x}{L}, \tag{12}$$

with $k_n = n\pi/L$, which in the discrete form becomes

$$\mathbf{T}\{f_j\} = \frac{2}{N_x}\mathbf{FST}\left\{F_n \frac{\hbar^2 k_n^2}{2m}\right\}. \tag{13}$$

The PiB representation formulated above is closely related to the PW method. In fact, for finite systems with soft-wall boundaries, the two representations are numerically equivalent. Mathematically, however, they are different: The PiB basis set is real and the zero boundary condition is imposed by the basis set itself, but in the PW case the basis functions are complex and the wave functions are forced to be zero at the boundaries by the external potential of systems under study. The PW method will fail in the case of the hard-wall boundary problem, which is quite common in the studies of quantum dots, but the PiB method is still valid. Mathematically the PiB method is closely related with the discrete variable representation methods that are widely used in chemical physics.[37]

C. Direct-minimization conjugate-gradient method for the Kohn-Sham equation

In direct-minimization approaches, the KS total-energy functional is minimized directly over orbital wave functions under orthonormal constraints.[22] We have made several important modifications to TPA's band-by-band conjugate-gradient scheme[30] to obtain higher efficiency. Here we give an outline of the algorithm, and emphasize the modifications we have made.

The basic idea of a band-by-band scheme is to minimize the total energy over one band (or orbital) at a time,[30] which, compared to other conjugate-gradient schemes,[38,39] has the following advantages: (1) much lower requirement for storage space, (2) simpler implementation, and (3) particularly in our algorithm, an efficient approximate line-minimization scheme, as will be shown.

First the steepest descent (SD) vector for the ith orbital at the mth iteration is calculated from

$$|\zeta_i^m\rangle = \left(1 - \sum_{j\neq i} |\psi_j\rangle\langle\psi_j|\right)(\lambda_i^m - \mathbf{H}_{\mathrm{KS}})|\psi_i^m\rangle \tag{14}$$

with $\lambda_i^m = \langle\psi_i^m|\mathbf{H}_{\mathrm{KS}}|\psi_i^m\rangle$ (to simplify the notation, we use Dirac's state vector notation and drop the spin index in the following formulation). In TPA's algorithm, the SD vector is preconditioned before it is used to build the conjugate vector. In our calculations, however, it was found that although in many cases preconditioning does accelerate the convergence, its effect is not always positive. On the other hand, the computational overhead in the preconditioning step, which involves another orthogonalization process as well as the action of the preconditioning operator on the SD vector, can be expensive for large systems. As shown later, by using a simplified multigrid technique, we can achieve fast convergence even without preconditioning of the SD vectors.

The conjugate vector $|\varphi_i^m\rangle$ is then constructed as a linear combination of the SD vector $|\zeta_i^m\rangle$ and the previous conjugate vector

$$|\varphi_i^m\rangle = |\zeta_i^m\rangle + \gamma_i^m|\varphi_i^{m-1}\rangle, \tag{15}$$

where

$$\gamma_i^m = \frac{\langle\zeta_i^m|\zeta_i^m\rangle}{\langle\zeta_i^{m-1}|\zeta_i^{m-1}\rangle} \tag{16}$$

with $\gamma_i^1 = 0$. The conjugate vector is further orthogonalized to the present band $|\psi_i^m\rangle$ and normalized ($\mathbf{N}$ is denoted as the normalization operator):

$$|\varphi_i'^m\rangle = \mathbf{N}(1 - |\psi_i^m\rangle\langle\psi_i^m|)|\varphi_i^m\rangle. \tag{17}$$

The new wave function for the ith orbital $|\psi_i^{m+1}\rangle$ is formed from the linear combination

$$|\psi_i^{m+1}\rangle = |\psi_i^m\rangle\cos\theta_{\min} + |\varphi_i'^m\rangle\sin\theta_{\min}, \tag{18}$$

which is guaranteed to remain normalized and orthogonal to all other orbitals. $\theta_{\min}$ is obtained by minimizing the total energy as a function of θ with $|\psi_i(\theta)\rangle = |\psi_i^m\rangle\cos\theta + |\varphi_i'^m\rangle\sin\theta$. In TPA's algorithm,[22,30] $\theta_{\min}$ is determined by the following approximate scheme: The total energy as a function of θ is approximated by $E(\theta) \approx E_{\mathrm{avg}} + A_1\cos 2\theta + B_1\sin 2\theta$; the three unknowns, E_{avg}, A_1 and B_1, are determined according to three pieces of information: $E(\theta=0)$, $\partial E(\theta)/\partial\theta|_{\theta=0}$, and $E(\theta=\pi/300)$.

Here we propose a more efficient approximate scheme for the determination of $\theta_{\min}$. The derivative of $E(\theta)$ with respect to θ can be obtained from

$$\frac{\partial E(\theta)}{\partial \theta} = 2\langle \varphi_i'^m | \mathbf{H}_{\mathrm{KS}}(\theta) | \psi_i^m \rangle \cos 2\theta - (\langle \psi_i^m | \mathbf{H}_{\mathrm{KS}}(\theta) | \psi_i^m \rangle - \langle \varphi_i'^m | \mathbf{H}_{\mathrm{KS}}(\theta) | \varphi_i'^m \rangle) \sin 2\theta. \tag{19}$$

Assuming $\mathbf{H}_{\mathrm{KS}}(\theta) \approx \mathbf{H}_{\mathrm{KS}}(0)$, from $\partial E(\theta)/\partial\theta = 0$ we get

$$\theta_{\min} = \frac{1}{2}\tan^{-1}\frac{B}{A} \tag{20}$$

with

$$A = -\langle \psi_i^m | \mathbf{H}_{\mathrm{KS}}(0) | \psi_i^m \rangle + \langle \varphi_i'^m | \mathbf{H}_{\mathrm{KS}}(0) | \varphi_i'^m \rangle \tag{21}$$

and

$$B = 2\langle \varphi_i'^m | \mathbf{H}_{\mathrm{KS}}(0) | \psi_i^m \rangle. \tag{22}$$

The underlying approximation in our scheme is similar to that of TPA's, but our scheme is much more efficient in terms of computational effort: In TPA's scheme, at each band iteration the total energy must be calculated twice, i.e., $E(\theta = 0)$ and $E(\theta = \pi/300)$; in our scheme, the most time-consuming step is the action of $\mathbf{H}_{\mathrm{KS}}$ on $|\varphi_i'^m\rangle$, which is much faster than the calculation of the total energy. Considering further the fact that the total number of band iterations can be very large, we note that an efficient line-minimization scheme such as ours is crucial to reduce the computational effort.

In TPA's algorithm, after the wave function is updated according to Eq. (18), the Kohn-Sham Hamiltonian is updated immediately, which involves the reconstruction of $V_H(\mathbf{r})$ and $V_{\mathrm{xc}}(\mathbf{r})$ according to the new density. This is actually quite expensive for large systems. On the other hand, we expect that the KS Hamiltonian will not experience large changes inside the iterations of a single orbital. So in our algorithm, we update $\mathbf{H}_{\mathrm{KS}}$ after every N_{update} band iterations, and the optimal value of N_{update} will be explored in the following section.

In each orbital, the procedure described above is repeated N_{band} times; the iterations are then started on the next orbital. After the wave functions of all orbitals are updated in this way, the total energy is calculated and is compared to that of the previous cycle to determine if the final convergence is achieved. The main parameters in the algorithm are N_{band} and N_{update}. Their effects on the performance of the algorithm will be tested in detail in the following section.

D. Calculation of V_H

For finite systems, the simplest and perhaps the most inefficient way to calculate V_H is by direct numerical integration, which is feasible only for small systems. Another widely used approach is to solve the Poisson equation equivalent to Eq. (5). Though the Poisson equation itself can be solved with great efficiency, the calculation of boundary values can be quite expensive even by using efficient multipole expansion techniques. Additionally, the Poisson solver approach is valid only for 3D systems; in the case of 2D systems, there is no Poisson equation equivalent to Eq. (5). In recent years, several schemes have been proposed to extend the conventional Fourier convolution method to finite systems.[26,28,29,40] In particular we have incorporated Martyna and Tuckerman's method[29] into our approach to quantum dots. Considering that the Martyna-Tuckerman method was developed mainly for the modeling of molecular and material systems within the plane-wave pseudopotential framework, we will formulate the approach here with some detail.

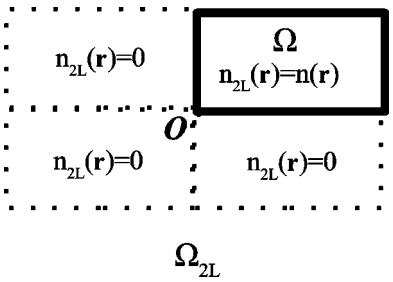

FIG. 1. Illustration of the Fourier convolution method for the calculation of the Hartree potential in finite systems. The original grid where the density and potential are defined is extended into doubled space. The density in the extended region is set to zero. Imposing the periodic boundary condition for this extended grid, the unphysical interaction between neighboring supercells can be avoided.

The calculation of the Hartree potential is straightforward for periodic systems, but this is not the case for finite aperiodic systems. The potential $V_H(\mathbf{r})$ has the form of the convolution between the density and the Coulomb interaction kernel, $v_c(\mathbf{r}) = 1/r$, which has the following simple relation in the Fourier space:[36]

$$\tilde{V}_H(\mathbf{k}) = \tilde{n}(\mathbf{k})\tilde{v}_c(\mathbf{k}), \tag{23}$$

where $\tilde{f}(\mathbf{k})$ refers to the Fourier transform of $f(\mathbf{r})$. Equation (23) is useful only when we have the analytical form of $\tilde{n}(\mathbf{k})$ and can perform the inverse Fourier transform of $\tilde{V}_H(\mathbf{k})$ analytically, which is not true for most cases where the density is usually represented in discrete real space.

When applying the Fourier method to discrete finite systems, periodic boundary conditions are always assumed. It has long been known that the unphysical interactions between neighboring supercells can be avoided by calculating V_H in a doubly extended grid.[41] In particular for 2D systems as illustrated in Fig. 1, the original $L_x \times L_y$ grid (Ω) is extended to $2L_x \times 2L_y$ (Ω_{2L}). The density in the extended grid is defined as

$$n_{2L}(\mathbf{r}) = \begin{cases} n(\mathbf{r}) & \text{if } \mathbf{r} \in \Omega \\ 0 & \text{otherwise.} \end{cases} \tag{24}$$

Imposing periodic boundary conditions to both the density and the Coulomb interaction kernel in the extended grid, the potential can be calculated according to the convolution theorem:

$$V_H(\mathbf{r}) = \sum_{\mathbf{k}} \overline{n}_{2L}(\mathbf{k}) \overline{v}_c(\mathbf{k}) e^{i\mathbf{k}\cdot\mathbf{r}}, \tag{25}$$

where $\overline{n}_{2L}(\mathbf{k})$ and $\overline{v}_c(\mathbf{k})$ are respectively finite Fourier integrals of the density and the Coulomb interaction kernel in the extended grid:

$$\overline{n}_{2L}(\mathbf{k}) = \frac{1}{\Omega_{2L}} \int_{\Omega_{2L}} n_{2L}(\mathbf{r}) e^{-i\mathbf{k}\cdot\mathbf{r}} d\mathbf{r}, \tag{26}$$

$$\overline{v}_c(\mathbf{k}) = \int_{\Omega_{2L}} v_c(\mathbf{r}) e^{-i\mathbf{k}\cdot\mathbf{r}} d\mathbf{r}, \tag{27}$$

where Ω_{2L} is used to denote both the extended grid and its volume (or area in the 2D case).

While $\overline{n}_{2L}(\mathbf{k})$ can be easily obtained from the discrete Fourier transform of its real-space values by FFT, the calculation of $\overline{v}_c(\mathbf{k})$ is much more involved because of the singularity of the Coulomb interaction kernel in real space. The key to Martyna-Tuckerman's approach is to decompose the Coulomb interaction kernel into long- and short-range parts:

$$v_c(\mathbf{r}) = \frac{\mathrm{erf}(\alpha r)}{r} + \frac{\mathrm{erfc}(\alpha r)}{r} \equiv v_c^{(\mathrm{long})}(\mathbf{r}) + v_c^{(\mathrm{short})}(\mathbf{r}), \tag{28}$$

where $\mathrm{erf}(x)$ and $\mathrm{erfc}(x)$ are the error function and its complement, respectively, and α is the parameter that controls the effective cutoff range. The finite Fourier integral of the short-range part can be well approximated by its infinite Fourier transform:

$$\begin{aligned} \overline{v}_c^{(\mathrm{short})}(\mathbf{k}) &\equiv \int_{\Omega_{2L}} v_c^{(\mathrm{short})}(\mathbf{r}) e^{-i\mathbf{k}\cdot\mathbf{r}} d\mathbf{r} \\ &\approx \int_{\text{whole space}} v_c^{(\mathrm{short})}(\mathbf{r}) e^{-i\mathbf{k}\cdot\mathbf{r}} d\mathbf{r} \equiv \tilde{v}_c^{(\mathrm{short})}(\mathbf{k}), \end{aligned} \tag{29}$$

which is analytically known in both 2D and 3D cases. The finite Fourier integral of the long-range interaction can be directly obtained from the discrete Fourier transform of its real-space values. In the practical implementation, $\overline{v}_c$ needs to be calculated only once at the beginning. The calculation of $V_H(\mathbf{r})$ involves only two FFT's (one forward and one backward), which makes this approach much more efficient than methods based on a Poisson solver.

E. Accelerating convergence: A one-way multigrid technique

The multigrid method is an efficient technique to accelerate the convergence in various real-space relaxation approaches.[36] The basic idea is that low-frequency errors are easier to eliminate on a coarse grid than on a fine grid. Lee *et al.*[31] proposed a simple one-way multigrid (OWMG) technique in finite-difference real-space KS calculations. Wave functions being represented in real space in our method, a similar technique can be implemented in a straightforward way: The KS energy functional is first minimized on a coarse grid; the converged wave functions, after interpolation and reorthogonalization, are taken as the initial guess for the minimization on the fine grid. With these well-preconditioned initial wave functions, the convergence on the fine grid can be easily attained.

III. NUMERICAL OPTIMIZATION OF PARAMETERS

Assembling all the pieces together, we test the performance and explore the optimal values of parameters of our method in a coupled quartic oscillator potential (QOP) system:

$$V_{\mathrm{ext}}(x,y) = a\left(\frac{x^4}{b} + by^4 - 2\lambda x^2 y^2 + \gamma(x^2 y - xy^2) r\right), \tag{30}$$

with $r = \sqrt{x^2+y^2}$. The prefactor a is used to control the e-e interaction strength, which is usually characterized by the Wigner-Seitz radius $r_s \equiv 1/\sqrt{\pi \overline{n}}$ with $\overline{n}$ being weighted average electron density, $\overline{n} = \int n^2(\mathbf{r}) d\mathbf{r}/N$. In this paper, we use $a = 10^{-4}$ to have $r_s \sim 1.5$, which is close to experimental values. The parameter b is usually taken as $\pi/4$. Both the classical dynamics and the single-particle quantum mechanics at $\gamma = 0$ have been extensively studied:[42] the system evolves continuously from integrable to fully chaotic as λ varies from 0 to 1. The parameter γ is introduced to break fourfold symmetry. In test calculations, we take $\lambda = 0.6$ and $\gamma = 0.1$.

The calculations are done in a grid of size $L_x = L_y = 50$ and the number of grid points is $N_x = N_y = 64$. All the numerical results in this section come from calculations with electron number $N = 100$ and spin $S = 0$. For the exchange-correlation energy E_{xc} we use Tanatar and Ceperley's parametrized form of the LSDA functional.[33] The convergence criterion is set as $\epsilon = 10^{-6}$, which corresponds to about 10^{-5} meV in GaAs-AlGaAs QD systems.

Considering that the FD method has been widely used in the numerical modeling of QD systems,[8,9,14,17] we first make a comparison between FD and PiB. In the FD representation, the second-order derivative in the kinetic-energy operator is locally discretized in real space:

$$\frac{\partial^2}{\partial x^2} f(x) = \frac{1}{h^2} \sum_{j=-m}^{m} C_j f_j + O(h^{2m}), \tag{31}$$

where h is the discretization step and the coefficients C_j can be obtained systematically for any m. Figure 2 shows the convergence of the total energy with respect to the number of grid points using 5-point ($m = 2$) FD, 13-point ($m = 6$) FD, and PiB representations. The low-order finite-difference scheme, $m = 2$, is poor in terms of accuracy, and converges slowly as the grid size increases. The high-order FD scheme, $m = 6$, improves the accuracy by two orders of magnitude, but is still less accurate than PiB for $N_x = 32$, 48, and 64.

We check the accuracy and efficiency of our line-minimization scheme by comparing with both TPA's approach and the numerically exact Brent's line search algorithm.[36] In this case, we use $N_{\mathrm{band}} = 5$ and $N_{\mathrm{update}} = 1$ as

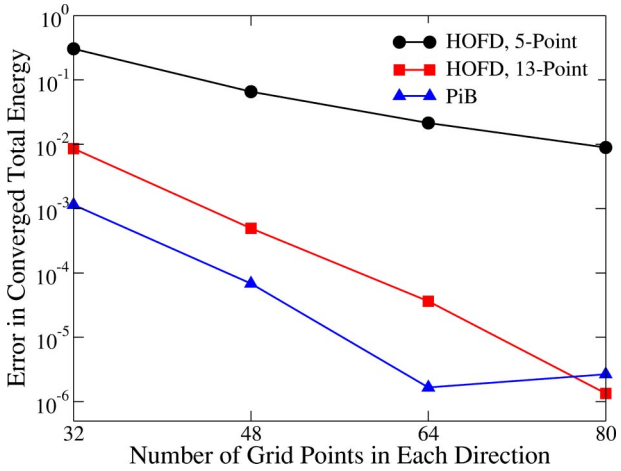

FIG. 2. (Color online) Convergence of the total energy with respect to the number of grid points using 5-point FD, 13-point FD, and PiB representation. We note that in the case of PiB, the error at $N_x=N_y=80$ is larger than that at $N_x=N_y=64$, which is mainly due to the numerical convergence error considering that the convergent criteria is taken as $\epsilon=10^{-6}$.

recommended in TPA's original work.[22] Figure 3 plots $\theta_{\min}$ in the first 25 band iterations calculated from the three schemes. The values of $\theta_{\min}$ from both TPA's and our method agree very well with exact values—the relative errors are always smaller than 1%. But in terms of computational effort, our scheme is much more efficient as discussed in the preceding section.

To find the optimal N_{band} and N_{update}, we do the calculations with different values of N_{band} and N_{update}, and the results are shown in Fig. 4. With fixed $N_{\text{update}}=1$, it is seen that a relatively larger N_{band} is more efficient than small N_{band}. Fixing $N_{\text{band}}=20$, $N_{\text{update}}=20$ gives the best performance. The combination of large N_{band} and N_{update} reduces the computational effort by almost one order of magnitude. Though the actual values of optimal N_{band} and N_{update} may vary for different systems, the basic idea demonstrated in this test calculation is believed to be of general significance.

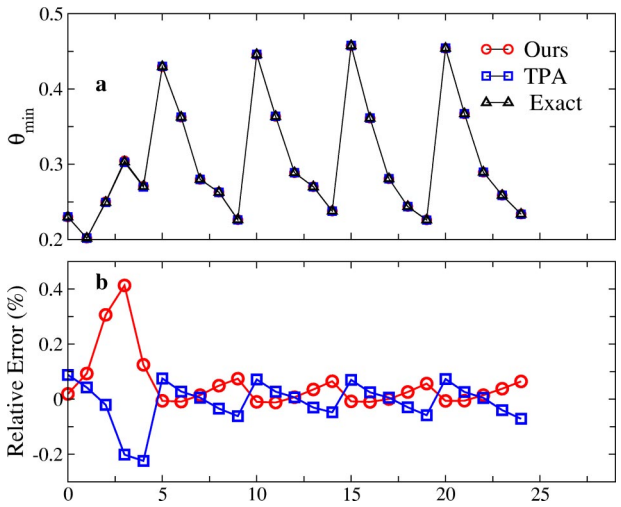

FIG. 3. (Color online) Comparison of $\theta_{\min}$ calculated by three different schemes.

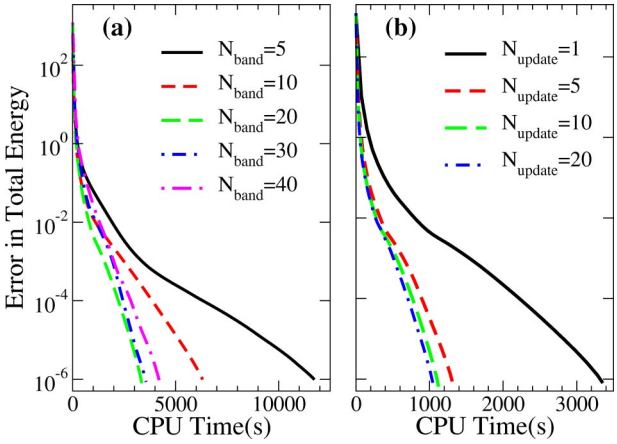

FIG. 4. (Color online) Errors in the total energy as a function of CPU time during the DMCG calculation for different N_{band} with $N_{\text{update}}=1$ (a) and for different N_{update} with $N_{\text{band}}=20$ (b) with respect to the exact total energy that is calculated using a finer grid ($N_x=80$) and tighter convergence criterion ($\epsilon=10^{-7}$).

We have implemented both the two-level (h and $2h$) and three-level ($h, \frac{4}{3}h$, and $2h$) OWMG schemes. Instead of using a sophisticated interpolation as in Ref. 31, we use a simpler Lagrange polynomial interpolation method. Comparison with the single-level calculation shows a quite obvious improvement in computational efficiency. To check the effect of the interpolation accuracy, in Fig. 5 we plot the relative computational effort in one KS calculation as a function of the order of the Lagrange interpolation formula in both two- and three-level OWMG calculations. We see that a high-order interpolation scheme is useful to improve the performance.

IV. APPLICATION: SPIN AND CONDUCTANCE PEAK-SPACING DISTRIBUTIONS IN LARGE INTEGRABLE AND CHAOTIC QUANTUM DOTS

In Coulomb blockade experiments of QD systems, the conductance through the dot varies strongly as a function of

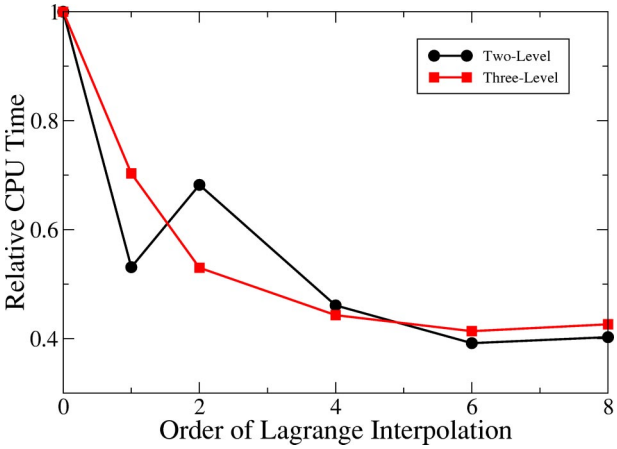

FIG. 5. (Color online) Relative computational efforts for one KS calculation as a function of the order of interpolation in both two- and three-level OWMG calculations. The CPU time in the single-level calculation is taken as the unit.

gate voltage, forming a series of sharp peaks.[1] In the linear regime at near-zero temperature, the spacing between neighboring peaks is related to the second difference of the ground-state energy $E_{\mathrm{g.s.}}$ with respect to electron number N:

$$\Delta_2 E(N) = E_{\mathrm{g.s.}}(N+1) + E_{\mathrm{g.s.}}(N-1) - 2E_{\mathrm{g.s.}}(N), \quad (32)$$

which is usually called the addition energy. The ground-state spin of the QD can be inferred from the shift in position of the conductance peaks upon applying a magnetic field. In small, highly symmetrical QD's with less than a few tens of electrons, the conductance peak spacing shows shell-filling structure, and the ground-state spin is determined by Hund's rule.[43] In large QD systems with irregular geometry or disorder, both quantities show random mesoscopic fluctuations, but their statistical properties are of universal significance.[1,2]

The connection between classical integrability and the quantum properties of noninteracting systems is well established.[44] When the classical dynamics is fully chaotic, the energies and wave-functions of a closed system follow the statistics of random matrix theory. In contrast, when the classical dynamics is integrable, there can be both larger and smaller spacings between the energy levels and distinctly nonrandom wave functions.

Here we are interested in the interplay between classical integrability and *e-e* interactions: Does the classical integrability of the external potential have significant effects on the statistical properties of quantum dots with *e-e* interactions fully considered? To answer this, we calculate spin and peak-spacing distributions in the QOP system in three different cases: fully integrable with fourfold symmetry ($\lambda=0, \gamma=0$), fully chaotic with symmetry ($\lambda=0.6, \gamma=0$), and fully chaotic without symmetry ($\lambda=0.6, \gamma=0.1$).[42] The high efficiency of our method makes it possible to calculate the ground-state energy and spin for N ranging from 1 up to 400, so that good statistics can be obtained from a *single* potential.

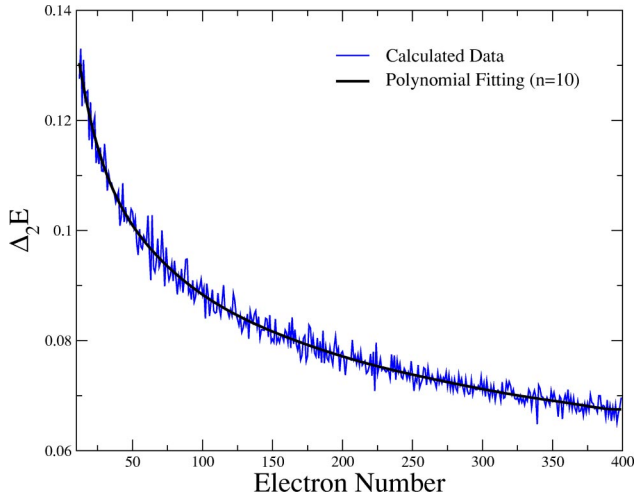

FIG. 6. (Color online) Addition energy as a function of N and its tenth-order polynomial fitting calculated from the QOP system with $\lambda=0.6, \gamma=0.1$. The overall trend is the classical effect of increasing charging energy as the quantum dot gets bigger while the fine structure is the quantum variation of interest.

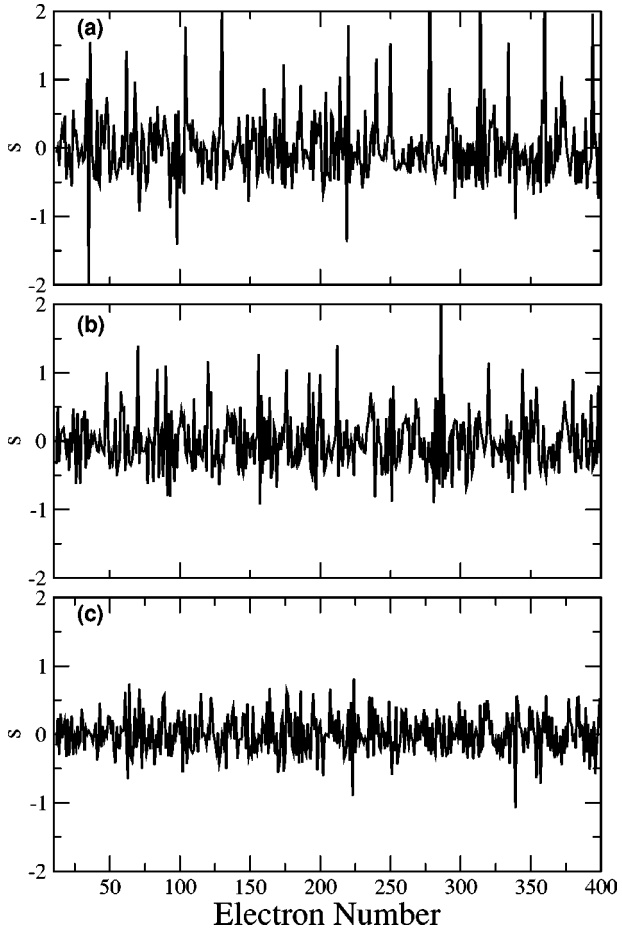

FIG. 7. Dimensionless peak spacing as a function of N in three different cases: (a) $\lambda=0.0, \gamma=0.0$ (integrable and symmetric); (b) $\lambda=0.6, \gamma=0.0$ (fully chaotic but symmetric); and (c) $\lambda=0.6, \gamma=0.1$ (fully chaotic and asymmetric).

For a given V_{ext}, the ground-state energy $E_{\mathrm{g.s.}}$ and spin $S_{\mathrm{g.s.}}$ as a function of N are determined by calculating several spin configurations for each N and selecting the one with minimum energy. As an example, Fig. 6 shows $\Delta_2 E(N)$ calculated in the potential ($\lambda=0.6, \gamma=0.1$). The spin distribution is simply the fraction of each spin configuration among all ground-state spins. To calculate the distribution of peak spacing, we need to first remove the smooth trend in $\Delta_2 E(N)$ (denoted $\overline{\Delta_2 E}$) as that is mainly a classical effect,[19] and scale the resultant data by the mean level spacing Δ. Δ is found from $\Delta = 2\pi\hbar^2/A_{\mathrm{eff}}$ with A_{eff} estimated as the classically allowed area at the Fermi level. The final dimensionless peak spacing, denoted s, is

$$s(N) \equiv \frac{\Delta_2 E(N) - \overline{\Delta_2 E}(N)}{\Delta}. \quad (33)$$

Probability distributions of s can be easily constructed; it is natural to look at the data when N is even separately from that when N is odd because of possible spin-degeneracy effects.

Figure 7 shows $s(N)$ in the three different cases. Note that

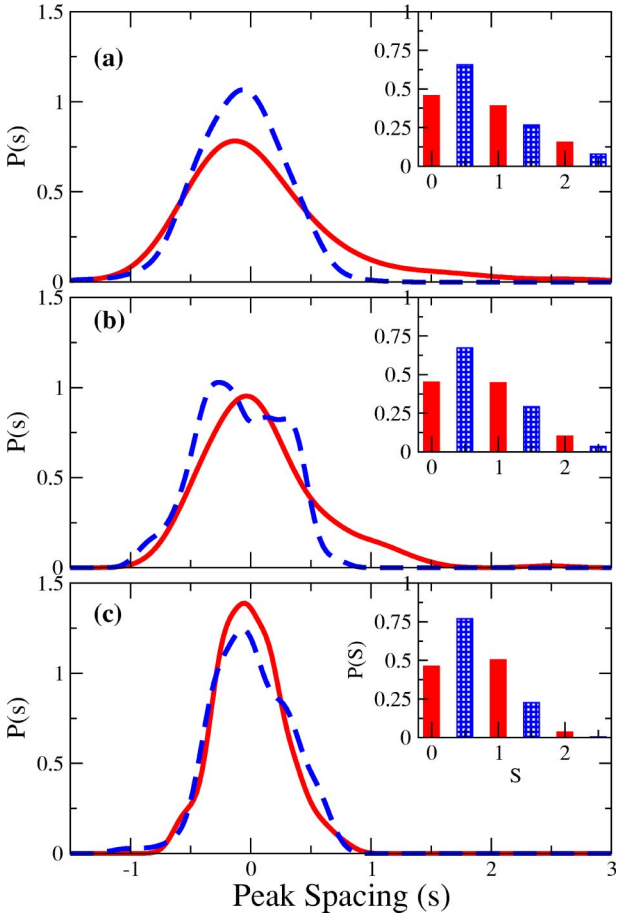

FIG. 8. (Color online) Peak-spacing distributions in N in three different cases: (a) $\lambda=0.0, \gamma=0.0$ (integrable and symmetric); (b) $\lambda=0.6, \gamma=0.0$ (fully chaotic but symmetric); and (c) $\lambda=0.6, \gamma=0.1$ (fully chaotic and asymmetric). The integrable symmetric case has the highest proportion of high-spin states and the largest difference between even N (solid, red) and odd N (dashed, blue). Insets: Distribution of ground-state spin in the three cases.

one can already see the difference between the cases in this raw data.

Figure 8 shows peak-spacing and ground-state spin distributions for even and odd N in the three cases. We call the reader's attention to several features: First, $P(s)$ is always fairly compact in the case of odd N but can have a long tail at large spacing for N even; this tail is caused by the energy of the top orbital when the spin sequence is $(\frac{1}{2}, 0, \frac{1}{2})$. Second, note the sharpness of $P(s)$ for $s \approx -0.5$ in panel (c) for both N even and odd. Third, there is a substantial probability of nonminimum spin. In fact, the probability of $S=0$ for N even is less than half in all three cases, and the fraction of dots with $S=\frac{3}{2}$ or 2 can be substantial. Finally, the probability of large ground-state spin decreases as the dot becomes less "regular" in terms of both classical dynamics and symmetry.

The most striking feature in Fig. 8, however, is the similarity between the case with integrable external potential and that with fully chaotic potential with the same geometrical symmetry. There are noticeable differences between the two cases—the distribution of peak spacing has longer negative and positive tails in the integrable case, for instance, reflecting the greater number of peaks in the raw data Fig. 7(a)—but on the whole both the peak-spacing and spin distributions are statistically the same and significantly different from those in Fig. 8(c). It seems that geometrical symmetry plays a more important role than the nature of the classical dynamics. A plausible interpretation of this feature is that the e-e interaction can break the classical integrability of the external potential more effectively than it can the symmetry—integrability is more fragile than symmetry.

V. SUMMARY

In this paper, we have presented an efficient method for the KS-SDFT simulation of large quantum dot systems. The main elements of the method are the following

(1) Wave functions are represented in real space, and the kinetic-energy operator is applied to wave functions by fast sine transform.

(2) The Hartree potential is calculated by Martyna and Tuckerman's Fourier convolution method.[29]

(3) For the solution of the KS equation, we introduced several important modifications to Teter *et al.*'s band-by-band conjugate-gradient method.[30] A more efficient approximate line-minimization scheme was developed; it was found that large band iteration number and a delayed update of the KS Hamiltonian inside the band iterations increase the efficiency by one order of magnitude.

(4) A one-way multigrid technique[31] was used to accelerate the convergence.

As an application of the method, we investigated the effects of the classical integrability of the external potential on spin and conductance peak-spacing distributions in a 2D model system with N up to 400. We found that the nature of the classical dynamics does influence the quantum properties of the interacting system, though not as much as the presence of symmetry in the external potential.

ACKNOWLEDGMENTS

We thank D. Ullmo for helpful discussions. This work was supported in part by NSF Grant No. DMR-0103003.

*Electronic address: baranger@phy.duke.edu
†Electronic address: weitao.yang@duke.edu

[1] L.P. Kouwenhoven, C.M. Marcus, P.L. McEuen, S. Tarucha, R.M. Wetervelt, and N.S. Wingreen, in *Mesoscopic Electron Transport*, edited by L.L. Sohn, G. Schön, and L.P. Kouwenhoven (Kluwer, Dordrecht, 1997), pp. 105–214.
[2] Y. Alhassid, Rev. Mod. Phys. **72**, 895 (2000).
[3] I.L. Aleiner, P.W. Brouwer, and L.I. Glazman, Phys. Rep. **358**, 309 (2002).
[4] S.M. Reimann and M. Manninen, Rev. Mod. Phys. **74**, 1283 (2002), and references therein.
[5] R.G. Parr and W. Yang, *Density-Functional Theory of Atoms and Molecules* (Oxford University Press, New York, 1989).
[6] R.O. Jones and O. Gunnarsson, Rev. Mod. Phys. **61**, 689 (1989).

[7] R.M. Dreizler and E.K.U. Gross, *Density Functional Theory: An Approach to the Quantum Many-Body Problem* (Springer-Verlag, Berlin, 1990).
[8] A. Kumar, S.E. Laux, and F. Stern, Phys. Rev. B **42**, 5166 (1990).
[9] M. Macucci, K. Hess, and G.J. Iafrate, Phys. Rev. B **48**, 17 354 (1993).
[10] D. Jovanovic and J.P. Leburton, Phys. Rev. B **49**, 7474 (1994).
[11] M. Stopa, Phys. Rev. B **54**, 13 767 (1996).
[12] S. Nagaraja, P. Matagne, V.Y. Thean, J.P. Leburton, Y.H. Kim, and R.M. Martin, Phys. Rev. B **56**, 15 752 (1997).
[13] M. Koskinen, M. Manninen, and S.M. Reimann, Phys. Rev. Lett. **79**, 1389 (1997).
[14] I.-H. Lee, V. Rao, R.M. Martin, and J.-P. Leburton, Phys. Rev. B **57**, 9035 (1998).
[15] S. Bednarek, B. Szafran, and J. Adamowski, Phys. Rev. B **64**, 195303 (2001).
[16] I.I. Yakimenko, A.M. Bychkov, and K.-F. Berggren, Phys. Rev. B **63**, 165309 (2001).
[17] M. Pi, A. Emperador, M. Barranco, and F. Garcias, Phys. Rev. B **63**, 115316 (2001).
[18] K. Hirose and N.S. Wingreen, Phys. Rev. B **65**, 193305 (2002).
[19] H. Jiang, H.U. Baranger, and W. Yang, Phys. Rev. Lett. **90**, 026806 (2003).
[20] D. Ullmo and H.U. Baranger, Phys. Rev. B **64**, 245324 (2001).
[21] G. Usaj and H.U. Baranger, Phys. Rev. B **66**, 155333 (2002).
[22] M.C. Payne, M.P. Teter, D.C. Allan, T.A. Arias, and J.D. Joannopoulos, Rev. Mod. Phys. **64**, 1045 (1992), and references therein.
[23] G. Kresse and J. Furthmüller, Phys. Rev. B **54**, 11 169 (1996), and references therein.
[24] A. Szabo and N.S. Ostlund, *Modern Quantum Chemistry* (McGraw-Hill, New York, 1989).
[25] J.R. Chelikowsky, N. Troullier, K. Wu, and Y. Saad, Phys. Rev. B **50**, 11 355 (1994).
[26] G. Onida, L. Reining, R.W. Godby, R. Del Sole, and W. Andreoni, Phys. Rev. Lett. **75**, 818 (1995).
[27] G. Makov and M.C. Payne, Phys. Rev. B **51**, 4014 (1995).
[28] M.R. Jarvis, I.D. White, R.W. Godby, and M.C. Payne, Phys. Rev. B **56**, 14 972 (1997).
[29] G.J. Martyna and M.E. Tuckerman, J. Chem. Phys. **110**, 2810 (1999).
[30] M.P. Teter, M.C. Payne, and D.C. Allan, Phys. Rev. B **40**, 12 255 (1989).
[31] I.-H. Lee, Y.-H. Kim, and R.M. Martin, Phys. Rev. B **61**, 4397 (2000).
[32] J.P. Perdew, K. Burke, and M. Ernzerhof, Phys. Rev. Lett. **77**, 3865 (1997).
[33] B. Tanatar and D.M. Ceperley, Phys. Rev. B **39**, 5005 (1989).
[34] C. Attaccalite, S. Moroni, P. Gori-Giorgi, and G.B. Bachelet, Phys. Rev. Lett. **88**, 256601 (2002).
[35] H. Saarikoski, E. Räsänen, S. Siljamäki, A. Harju, M.J. Puska, and R.M. Nieminen, Phys. Rev. B **67**, 205327 (2003).
[36] W.H. Press, B.P. Flannery, S.A. Teukolsky, and W.T. Vetterlin, *Numerical Recipes: The Art of Scientific Computing* (Cambridge University, Cambridge, England, 1989).
[37] J.C. Light and T. Carrington, Jr., in *Adv. Chem. Phys.*, edited by I. Prigogine and S.A. Rice (Wiley, New York, 2000), p. 263.
[38] I. Stich, R. Car, M. Parrinello, and S. Baroni, Phys. Rev. B **39**, 4997 (1989).
[39] M.J. Gillan, J. Phys.: Condens. Matter **1**, 689 (1989).
[40] L.M. Fraser, W.M.C. Foulkes, G. Rajagopal, R.J. Needs, S.D. Kenny, and A.J. Williamson, Phys. Rev. B **53**, 1814 (1996).
[41] R.W. Hockney, Methods Comput. Phys. **9**, 135 (1970).
[42] O. Bohigas, S. Tomsovic, and D. Ullmo, Phys. Rep. **223**, 43 (1993).
[43] L.P. Kouwenhoven, D.G. Austing, and S. Tarucha, Rep. Prog. Phys. **64**, 701 (2001).
[44] M.C. Gutzwiller, *Chaos in Classical and Quantum Mechanics* (Springer-Verlag, New York, 1990).